IEE

PROCEEDINGS-C

Generation, Transmission and Distribution

July 1981 Volume 128 Part C Number 4

UK ISSN 0143–7046 IPPDDA 128 (4) 177–252

Contents

Dynamic analysis of lightly iced conductor galloping in two degrees of freedom

A.S. Richardson, Jr., B.Sc., M.Sc., Sen. Mem. I.E.E.E.

Indexing terms: *Cables and overhead lines, Power transmission, Power systems and plant*

Abstract: Field observations have been repeatedly reported on the galloping of transmission lines having only a small acretion of ice of the order of 10% of the diameter on the windward side. Aerodynamic force measurements in wind tunnels reveal that significant lift forces are present, having a steep gradient with respect to angle of attack, and which satisfy the Den Hartog negative damping criteria. Drag forces are essentially constant, and aerodynamic moments are zero over the 360° range of angle of attack. Similarly, no unbalanced inertia forces exist for such light-ice deposits, which precludes the dynamic inertia coupling between galloping and torsion modes.

Blow back of the conductor is shown to explain such galloping owing to the angle of attack reaching the critical range, within a finite range of wind speed. The addition of control devices, identified as the windamper, and the detuner, is shown to modify the distribution of angle of attack along the span, thus altering the angle of attack 'exposure' compared with that of an untreated span. Stability analyses in two degrees of freedom (galloping and dynamic twist) are performed for a number of representative cases. Stability is expressed as the root locus of a fourth-degree polynomial (quartic) equation, as a function of wind speed. Perforated cylinder dampers are also considered, and they are found to supply inadequate damping for control, unless the span coverage is unreasonably large. The twisting effect of the Windamper is shown to be its primary stabilising influence. The detuner appears to increase the range of instability in two out of three cases.

List of symbols

C_L = lift coefficient (dimensionless, based on conductor diameter)
$C_{L\alpha}$ = lift coefficient slope with angle of attack
α = local angle of attack
C_D = drag coefficient (dimensionless, based on conductor diameter)
C_α = Den Hartog coefficient ($C_D + C_{L\alpha}$)
β_0 = blow-back angle, untreated span (eqn. 1), rad
β = blow-back angle, treated span (eqn. 2), rad
q = dynamic pressure of wind
d = conductor diameter
mg = conductor weight per unit of span length
g = acceleration due to gravity
U = wind speed
ρ = air density
D_1 = aerodynamic drag of damper
W_1 = deadweight of control device
l = semispan length of conductor span
M = control device mass
I = control device moment of inertia about conductor axis
GJ = torsion stiffness of conductor per unit span length
a = distance of device CG from conductor axis
θ = blow-out angle of windamper (Fig. 7)
K^*_θ = windamper aerodynamic stiffness
$d\Sigma/d\theta$ = slope of windamper moment parameter (Fig. 8)
$\sum$ = moment parameter for windamper
ϕ = dynamic twist angle (Fig. 9)
ω_ϕ = natural torsion frequency of device, rad/s
ζ_ϕ = damping in torsion for windamper
y = vertical amplitude of galloping mode
ω_y = natural frequency of galloping mode, rad/s
x = span co-ordinate measured from midspan
f_y = mode-shape function of galloping mode
ζ_y = aerodynamic damping ratio of galloping mode
ζ_0 = damping ratio of galloping mode at zero airspeed
U_c = critical galloping wind speed
C'_α = effective spanwise Den Hartog coefficient
ζ^*_D = effective span damping ratio for device
C^*_α = Den Hartog coefficient for damper, based on damper area
ζ = sum of aerodynamic damping ratios
x_θ = dimensionless eccentric moment coupling parameter
Z = characteristic length parameter based on dynamic pressure
s_θ = dimensionless eccentric moment coupling parameter
R = ratio of torsion to galloping natural frequencies
$C'_{L\alpha}$ = effective spanwise lift coefficient slope
f_ϕ = torsion mode shape function along span
$C^*_{L\alpha}$ = lift curve slope of damper, based on damper area
r = span cover factor for aerodynamic damper
t = time, s
v_y = eigenvector in y due to ϕ
v_ϕ = eigenvector in $\dot{\phi}$ due to y

Paper 1379C, first received 20th May and in revised form 25th November 1980

The author is with Research Consulting Associates, 3 Wingate Road, Lexington, MA 02173, USA

1 Introduction

Recent developments in the field of galloping-conductor technology have encompassed a wide spectrum of engineering and practical approaches. A new reference book [1] includes an up-to-date summary of a number of methods that have been applied, mainly on an experimental basis, during the past 15 years. These methods include electrical permutation of circuits [2], unbundling of bundled conductors [3], interphase spacers [4], and the application of several device concepts for galloping control [5, 6, 7].

In addition, advances have been made in the theoretical approach to galloping. Some of these have concerned the maximum possible galloping amplitude [8], and have resulted in very crude predictions of amplitude dependency on wind speed. That particular theory is based on energy-balance principles, but also aerodynamic nonlinear coefficients of lift in the range bounded by ± 0.6 as in a step function. Although that characterisation is greatly different from the wind-tunnel measurements of lift coefficient on 'typical' ice-shaped models, the maximum reported galloping amplitudes by the EEI Galloping Task Force in 66 reported cases exceed the value calculated by the theory [8] in only 9% of the cases [1]. It appears that the compelling simplicity of this result should guarantee its continued usage. However, the theory seems to break down when it is applied to aerodynamic dampers,

0143-7046/81/040211 + 08 $01.50

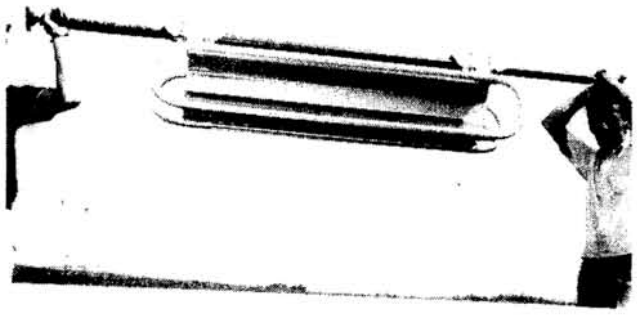

Fig. 1 *Windamper*

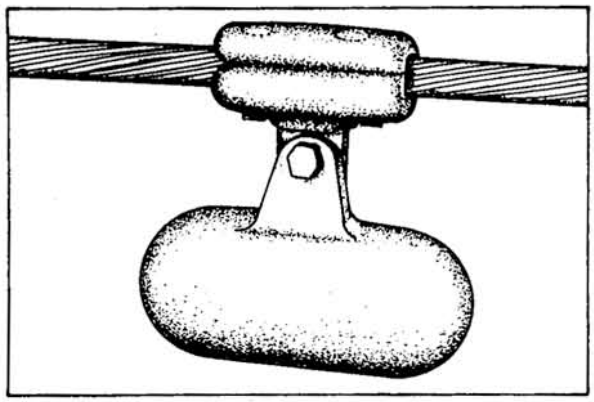

Fig. 2 *Detuner pendulum*

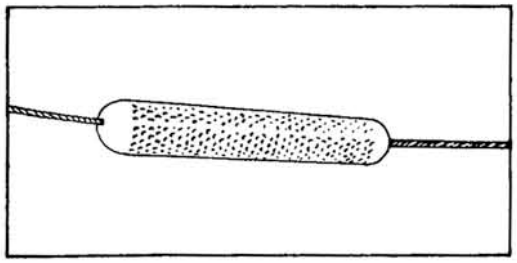

Fig. 3 *Perforated cylinder damper*

predicting only modest reduction in galloping amplitudes, whereas field observations indicate significantly reduced amplitudes [9]. One objective of this paper is to explain why this is so.

Another theory which has appeared within the past five years is the torsional 'detuning' theory. Here, the fundamental notion is that a matching of the conductor torsional mode frequency with one of the lower galloping mode frequencies due to ice and wind effects is the cause of galloping [10]. In the detuning theory a remedy is proposed for control, consisting of a discrete number of 'detuner pendulums' that are to be attached along the span. One puzzling aspect of this theory is that it cannot be reconciled with the predominance of galloping cases reported under lightly iced conductors [1], where ice thickness is less than 0.25 cm. For such light-ice coatings the effects on the conductor torsion natural frequency are negligibly small, as are the effects of the static unbalance due to ice. The mechanism for coupling between torsion and galloping in such cases is nonexistent in single conductors, and in bundled conductors is difficult to visualise even though, in the latter, the torsion and galloping frequencies may be almost matched. Yet this method has received such widespread attention that an in-depth analysis of it seems warranted. That is a second objective of the paper.

The final theory, which is the primary objective of the paper, is one based on the original Den Hartog theory, but including the effects of spanwise twisting [11]. Here, that theory will be extended to include the coupled motions of torsion and galloping, especially due to the added control devices. No nonlinearities are considered. Stability or instability is judged solely on the basis of the sign of the mode damping ratio: stable if positive, unstable if negative. Here, the mode damping ratio is found from the solution of a quartic equation, whose roots are the eigenvalues for the coupled system. In control theory terminology, the question is: are there any poles (roots) in the left half plane?

As a practical matter, and to illustrate the method, a typical conductor span of Drake single conductor on 277 m span at 20% UBS* tension is considered subject to a coating of light ice. The untreated span is compared to treated spans, having, in turn, detuner pendulums, perforated cylinder dampers, and windampers. Attachment points, in all cases, are the two one-third points in the span. For a consistent comparison, detuner and windamper eccentric mass and moment of inertia are equal, and perforated cylinder damper and windamper drag are equal up to 64 km/h wind speed.

Three initial orientations of the light-ice shape are considered. One with $\alpha_0 = 0$ corresponds to ice accretion directly to windward. The other two, having $\alpha_0 = 10°$ and $\alpha_0 = -10°$, respectively, refer to ice accretion slightly above or slightly below a horizontal plane.

Although the developed theory is applied to a specific illustrative example, the notation is generalised to afford application to any single-conductor problem having a light-ice profile.

2 Description of conductor used for the illustration of the method

The standard Drake conductor (54/7 ACSR) is used to illustrate the necessary considerations, see Table 1.

Table 1: Conductor specification

Type:		54/7 ACSR	Drake 795 MCM	
Overall diameter	=	1.093 in	(27.76 mm)	
UBS	=	28 500 lbs	(12,950 kgf)	
Weight	=	1.09 lb/ft	(1.61 kg/m)	
Torsion stiffness	=	1045 lbft²/rad		(432 Nm²/rad)
Tension	=	5,800 lb	(2636 kgf)	(20% UBS)
Span	=	900 ft	(277 m)	
Moment of inertia	=	0.17 lbin²/ft		(1.65 kgcm²/m)
Sag	=	19 ft	(5.85 m)	
1st mode frequency	=		0.23 Hz	(1.44 rad/s)
2nd mode frequency	=		0.46 Hz	(2.88 rad/s)

3 Initial conditions with light ice

The entire span is assumed to be coated with light ice havin a thickness of 0.1 in (0.25 cm), and a crescent shape formed o the windward side. The aerodynamic characteristics wer found in wind-tunnel tests [12], and also later reported in CIGRE paper [13]. For the purpose of analysis, the dra coefficient is assumed constant at a value of unity, the momen coefficient is assumed zero, and the lift coefficient C_L th lift coefficient slope $C_{L\alpha}$, and the Den Hartog coefficien $C_\alpha = C_D + C_{L\alpha}$ are represented by analytical approximatio [11]. The latter two, used in the present analysis, are ind

UBS = ultimate breaking strength

cated in Fig. 4. The angle of attack, measured positive clockwise with the wind from the left, is considered as zero when the axis of symmetry of the crescent is in a horizontal plane. Both the C_α function and the $C_{L\alpha}$ function are even functions of α. For an angle of attack greater than 40°, $C_\alpha = C_D = 1.0$

Notice that the C_α function can reach positive values of + 3, but the negative limit is − 1. This comes into play in a twisted conductor, and has a profound effect on the stability of the span.

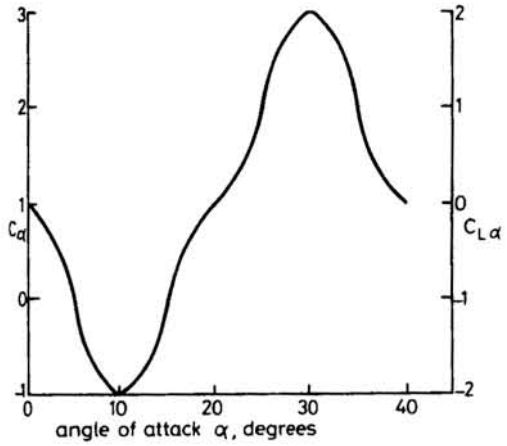

Fig. 4 *Aerodynamic coefficients for light ice*

Because the ice coating is light, no change is assumed in the conductor polar moment of inertia, and the aerodynamic moment is considered zero. The angle of attack range in which C_α is negative is from 5° and 15°. The ice shape can reach this condition (and may become unstable) when the conductor blow-back angle β_0 comes within that range. For small angles,

$$\beta_0 = C_D\, q\, d/mg \qquad (1)$$

where

d = conductor diameter

q = dynamic wind pressure ($\rho U^2/2$)

ρ = air density = 1.23 kg/m^3

U = wind speed

mg = conductor weight per unit length

For the Drake conductor, the blow back at 32 km/h wind speed is about 4.8°, which is in the stable range of C_α. At 40 km/h the blow back is 7.5°, and, since C_α is negative, the conductor may gallop. If the initial angle α_0 of ice formation is different from zero, then different wind speeds are required to reach the range of negative values. Further, the addition of certain types of control devices will change the blow-back picture somewhat.

In the case of either the Windamper or the perforated cylinder the blow back is*

$$\beta = [\beta_0 + (4/3)(D_1/mgl)]\,/\,[1 + (8/3)W_1/mgl] \qquad (2)$$

where

D_1 = aerodynamic drag of device

l = semispan length

W_1 = weight of device

For comparison purposes, the perforated cylinder is assumed to have the same drag as the windamper, and the same weight. Also both are assumed located at each of the one-third span points.

The lastest version of the perforated cylinder has a length of 3.05 m and a mass per unit length of 3.52 kg/m [14]. This compares on an equal weight basis with a 1.2 m – length windamper. The comparison on the basis of drag is also correct if it may be assumed that the perforated cylinder develops a drag coefficient of 1.15, as against the drag coefficient of the windamper of 2.15.

In the case of the detuner pendulum, there is no drag, but the weight is assumed equal to that of the windamper, i.e. 22 lb (10 kg).

The blowback is shown in Fig. 5 for the various cases to be considered. In the case of the perforated cylinder damper, it is assumed here to be attached concentrically with the single conductor axis. This is somewhat at variance with the use it has seen on bundled conductor to date, but, in the present comparison, the use of a little imagination could interpret the results for it in terms of a bundled-conductor application as well. No bundled-conductor applications are considered here for either the windamper or the detuner pendulum, however.

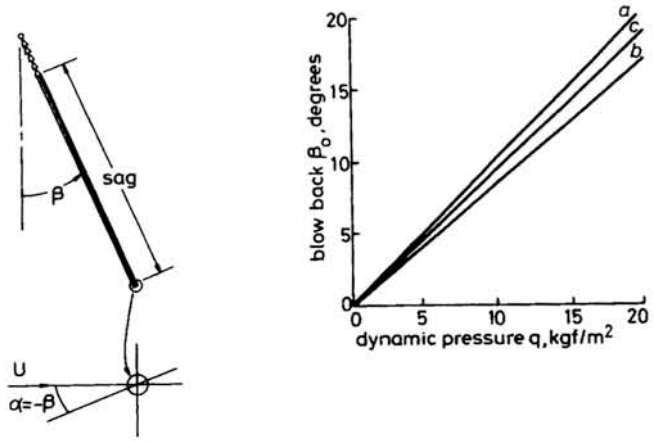

Fig. 5 *Conductor blow-back angle*

a Windamper and cylinder
b Detuner pendulum
c Untreated span

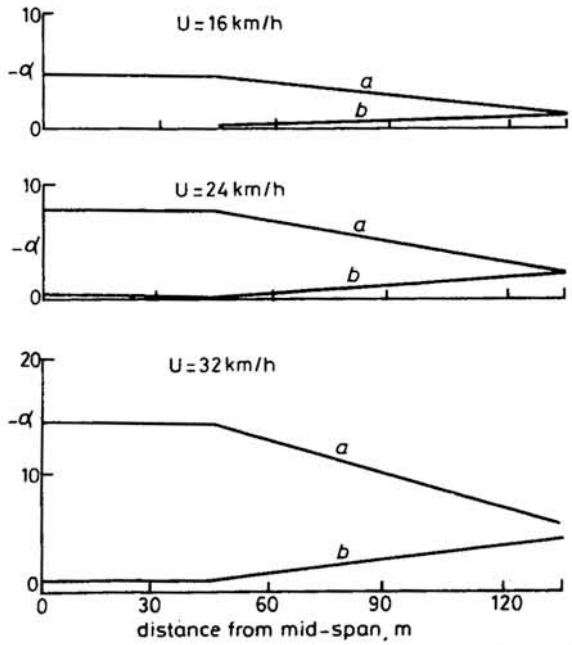

Fig. 6 *Angle of attack distribution along span for windamper and detuner*

a Windamper *b* Detuner
Total span = 274 m; Drake conductor; 1/3 span attachment for device units
Axis of symmetry of ice shape is initially horizontal ($\alpha_0 = 0$)

*The catenary is assumed to have a parabolic shape.

It is seen that the dead weight of the units reduces the blow back by approximately 12%, but the aerodynamic units tend to increase the blow back according to dynamic wind pressure. At a wind speed of 40 km/h the blow-back angles are 6.7° for the detuner, 7.5° for the untreated span, and 8.3° for the aerodynamic units. However, there is more to consider.

As the conductor blows back with the devices attached to the one-third span points, the offset pendulum weight applies a twisting moment which twists the conductor, clockwise according to our convention, thus limiting the angle-of-attack change due to blow back. On the other hand, the windamper by its action twists the conductor in a counterclockwise direction, thus increasing the angle-of-attack change locally. Contrary to this, the perforated cylinder just blows back with the conductor, the angle of attack being $\alpha = -\beta$, and constant along the span. The angle of attack distributions along the semispan for the windamper and the detuner pendulum are shown in Fig. 6, for three wind speeds. These are symmetrical about midspan. In the case of the windamper, the centre one-third span blows out according to Fig. 7 [11].

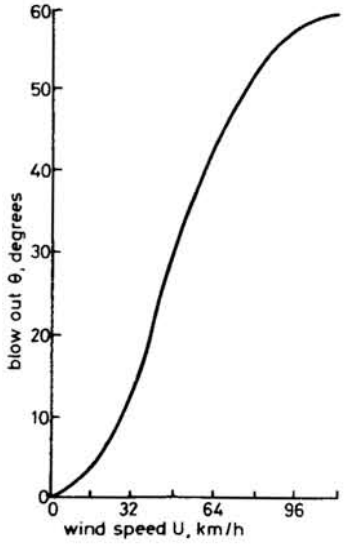

Fig. 7 *Windamper blow out for Drake conductor*

4 Dynamic twisting

As a part of establishing initial conditions, the dynamic twisting, including the effects of the devices, must be established.

There are two modes to consider:

(*a*) in-phase twisting when the devices located at the one-third points move in phase with each other

(*b*) out-of-phase twisting when the devices move in anti-phase.

The latter has the higher frequency.

Zero air speed case: When there is no wind, the dynamic twisting of the windamper and the detuner pendulum are identical. Also, it is easily established that the kinetic energy of the twisting conductor mass is less than 1% of the kinetic energy of the moving devices except when the devices form a nodal point, the latter being the third torsion mode having a frequency outside the range of concern. Accordingly, the in-phase mode natural frequency is given by eqn. 3*a*, and the out-of-phase, natural frequency by eqn. 3*b*:

$$\omega_\phi = \sqrt{\frac{Mga + GJ/2l/3}{I}} \tag{3a}$$

$$= \sqrt{\frac{Mga + GJ/2l/3 + GJ/1l/3}{I}} \tag{3b}$$

where

Mg = device weight (10 kg)

I = device moment of inertia about conductor

GJ = conductor torsion stiffness

a = distance from device CG to conductor

The calculated frequencies are 6.11 rad/s and 6.95 rad/s respectively.

Effect of wind: There is no effect of wind on the detuner natural frequencies, but there will be an effect on the windamper owing to the blow out of it and the aerodynamic stiffness of it. The blow out effect is accounted for by replacing Mga by $Mga\cos\theta$, and θ varies as in Fig. 7. The aerodynamic stiffness is accounted for by the sigma parameter [11] shown in Fig. 8. This results in an 'effective' stiffness for the windamper amounting to

$$K_\theta^* = -aqd\Sigma/d\theta \tag{4}$$

In this expression the slope of the sigma curve is a function of the wind speed.

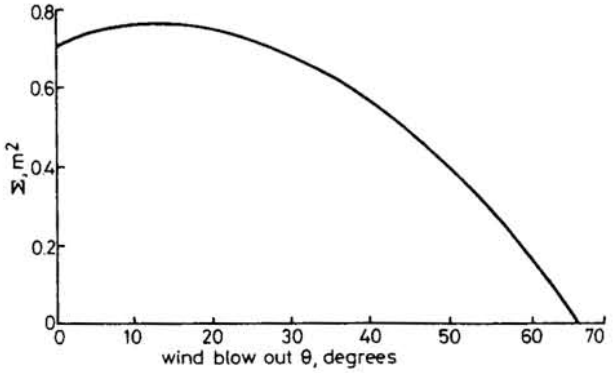

Fig. 8 *Aerodynamic moment parameter* Σ *(1.2 m damper)*

The torsion natural frequencies, including the 'effective' windamper stiffness, are shown in Table 2. The first column shows the in-phase frequencies, and the second shows the out-of-phase frequencies. Notice a slight reduction in numerical value at low wind speed corresponding to the positive slope of the sigma parameter for small blow-out angles, Fig. 8.

Table 2: Windamper torsion frequencies

Wind speed	Frequency		K_θ^*
km/h	rad/s		m/rad
0	6.11	6.95	−1.3
16	5.99	6.85	−0.8
24	6.04	6.89	+2.8
32	6.34	7.15	10.8
40	6.95	7.70	20.8
48	7.76	8.44	34.2
56	8.65	9.27	53.2
64	9.79	10.33	82.2
72	11.29	11.77	112.2

In the case of the detuner, the frequencies are constant the zero wind speed values.

With reference to Fig. 9, dynamic twisting motion ϕ considered, first, without any coupling to the y co-ordin and governed by the differential equation

$$I\ddot{\phi} + I\omega_\phi^2\phi = qad\Sigma/d\theta\,(a\dot{\phi}/U)\sin\theta$$

where the aerodynamic twisting moment on the right-ha side is seen to be proportional to the angular velocity.

rearranging terms, this may be put into the standard form:

$$\ddot{\phi} + 2\zeta_\phi \omega_\phi \dot{\phi} + \omega_\phi^2 \phi = 0 \tag{6}$$

where

$$\zeta_\phi = -qa^2 \sin\theta \, (d\Sigma/d\theta)/2UI\omega_\phi$$

the latter being the damping ratio in the torsion mode. It is seen to be proportional to wind speed, and to the aerodynamic sigma parameter. Since the latter always has negative slope with θ over the range of wind speed of practical interest, the damping is always positive. At 48 km/h the damping ratio is about 2%. In the case of the detuner pendulum, the damping ratio is assumed zero.

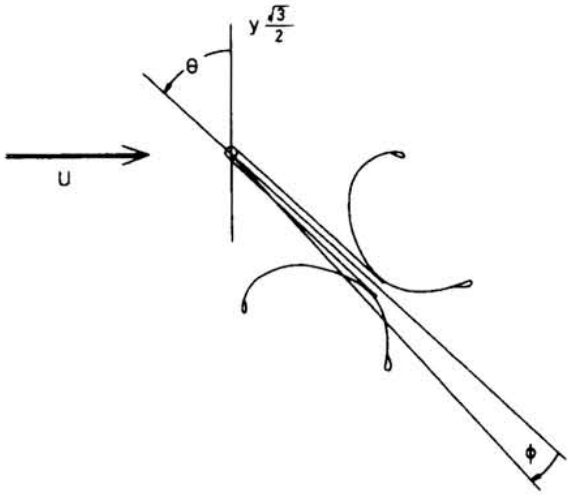

Fig. 9 *Generalised co-ordinates*

5 Single-degree-of-freedom vertical motion

The differential equation for the uncoupled vertical motion in either the first mode or the second mode is [11, 12]

$$\ddot{y} + \omega_y^2 y = -(qd\dot{y}/mlU) \int_{-l}^{l} C_\alpha f_y^2 \, dx \tag{7}$$

where $f_y = \cos(\pi x/2l)$ for the first mode, and $= \sin(\pi x/l)$ for the second mode, d = conductor diameter, and m = mass per unit length. The natural frequency ω_y, is chosen according to the mode number.

In this form, it is assumed that the aerodynamic coefficient C_α can vary along the span, as for the case of either the windamper or the detuner pendulum. In the case of the untreated span or the perforated cylinder damper, it is constant along the span, and the integral in eqn. 7 becomes C_α. On rearranging terms, the equation becomes

$$\ddot{y} + 2\zeta_y \omega_y \dot{y} + \omega_y^2 y = 0 \tag{8}$$

where the mode damping ratio is

$$\zeta_y = (qd/2mlU\omega_y) \int_{-l}^{l} C_\alpha f_y^2 dx$$

Hence galloping is defined whenever the average weighted aerodynamic coefficient is negative. In general, it is seen that, when C_α varies along the span, its integrated weighted average depends on mode number. The form of eqn. 8 is convenient to use when the mechanical damping ζ_0 of the span is known, because it can be added algebraically to ζ_y, resulting in the critical wind speed

$$U_c = -4\zeta_0 m\omega_y/\rho d C'_\alpha \tag{9}$$

and C'_α is defined as the integrated weighted average of C_α, and ρ = air density

$$C'_\alpha = (1/l) \int_{-l}^{l} C_\alpha f_y^2 \, dx \tag{10}$$

In the case of either the windamper or the detuner pendulum, it has already been seen how the angle of attack varies along the span as in Fig. 6. This is used with Fig. 4 to obtain the distribution of the C_α coefficient along the span, then weighted according to eqn. 10. In the case of the untreated span or the perforated cylinder damper, since $\alpha = -\beta$ then eqn. 10 reduces to $C'_\alpha = C_\alpha(-\beta)$.

In the case of either the windamper or the perforated cylinder damper, there is an additional term to consider in eqn. 8 that is additive to the second term and may be identified by the damping ratio of the damper itself,

$$\zeta_D = (3/4) q C^*_\alpha A_w / 2ml\omega_y U \tag{11}$$

where

C^*_α = aerodynamic coefficient of the damper

A_w = total projected area of all dampers

The factor of 3/4 appears owing to the location of the damper at the one-third points (see Fig. 9). The total area of all dampers used in the span follows from the form of eqn. 7, and the application of the integral to the damper at the appropriate span location.

In the case of the windamper, at 48 km/h the damping ratio according to eqn. 11 is about 2% in the first mode and 1% in the second, based on a numerical value of C^*_α of 3.65 [11]. In the case of the perforated cylinder damper, C^*_α is just equal to its drag coefficient of 1.15, but its projected area is 2.5 times that of the windamper, resulting in first- and second-mode damping ratios of 1.6% and 0.8%, respectively, at 48 km/h. As the span mechanical damping ratio is probably

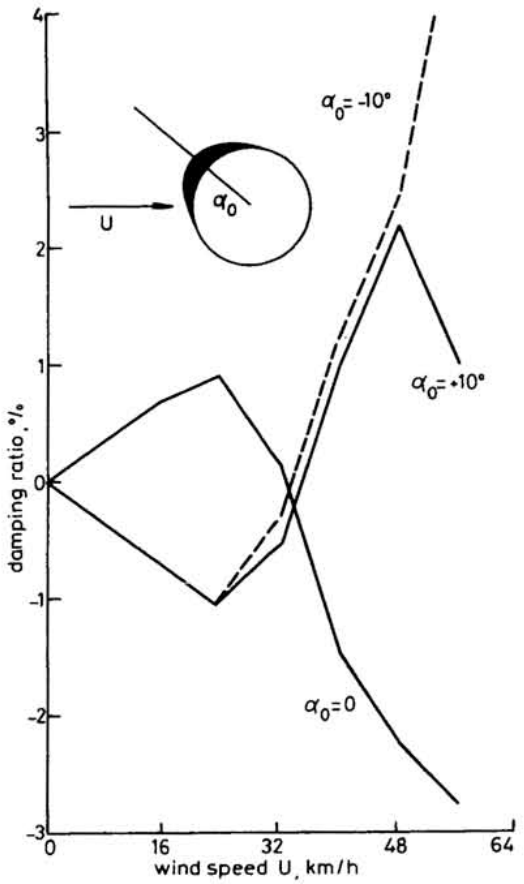

Fig. 10 *Untreated span damping ratio: second mode*

not more than 0.5%, it is apparent that both devices add significant amounts of damping. Detuner pendulums, of course, add no damping to the span.

For the purpose of illustration, then, three different cases for the untreated span are shown in Fig. 10. The three cases are for three different initial angles of attack of the light-ice shape. It is seen that all three will become unstable, but in differing ranges of wind speed. For $\alpha_0 = 0$, the instability occurs only above 35 km/h ($\zeta_0 = 0.5\%$, assumed), but, for $\alpha_0 = \pm 10^\circ$, the instability occurs in the range of 12–32 km/h. Further, it is clear that neither of the two aerodynamic dampers can supply sufficient damping. This shows that if the windamper is fixed in the span so as not to twist the conductor, its control capability would be little better than the perforated cylinder. Furthermore, a heavy windamper such as the units under experimental investigation by Ontario Hydro in Canada, may not be a good idea either. Thus, the reason for the windamper's success on single-conductor spans is clearly not its damping ability alone. Some other effect must be responsible, and it appears to be strongly related to the twisting of the conductor.

6 Dynamic analysis in two degrees of freedom

The differential equations of motion for a coupled system have been derived for a continuous span having aerodynamic coefficients which do not vary along the span [12]. These may be easily modified to include such variations, and also the dynamic effect of the windamper:

$$\begin{aligned} &\ddot{y} + 2\zeta\dot{y} + y - x_\theta Z\ddot{\phi} - (C'_{L\alpha} + rC^*_{L\alpha})Z\phi \\ &\quad - (\omega_y a \sin\theta/U) rC^*_\alpha Z\dot{\phi} = 0 \\ &\quad - s_\theta \ddot{y} - \sqrt{3}\, R(\zeta_\phi/\sin\theta)\dot{y} \\ &\quad + a\ddot{\phi} + 2\zeta_\phi Ra\dot{\phi} + R^2 a\phi = 0 \end{aligned} \tag{12}$$

where

$$\begin{aligned} \zeta &= \zeta_y + \zeta_D \\ x_\theta &= \sqrt{3/4}\, Ma \sin\theta/mlZ \\ r &= \sqrt{3/4}\, A_w/dl \\ Z &= qd/\omega_y^2 m \\ s_\theta &= \sqrt{3/4}\,(Ma^2/I)\sin\theta \\ R &= \omega_\phi/\omega_y \\ C'_{L\alpha} &= \int_{-1}^{1} C_{L\alpha} f_y f_\phi d(x/l) \end{aligned}$$

The first of eqns. 12 indicates static and dynamic coupling, and viscous coupling through the damper. The second equation indicates only dynamic and viscous coupling. The strength of the coupling depends on the span cover factor r, the blow out θ, and the dynamic pressure term here expressed as a characteristic length Z. Time is replaced by $\omega_y t$. The lift-curve slope of the damper is $C^*_{L\alpha} = 1.5$.

These equations are solved in the classical way by assuming solutions of the form $\exp(pt)$, which leads to a quartic equation in p. A convenient method of obtaining the roots of the quartic is Lin's method [15]. The roots found in this way are found to differ from the uncoupled roots only in the damping ratio, the frequencies remaining as in the uncoupled modes. Further, only the first vertical mode is influenced by the in-phase torsion, and only the second vertical mode is influenced by the out-of-phase torsion. The detuner pendulum does not couple dynamically owing to its small values for θ. Its primary influence is on the aerodynamic damping of the y mode. This is shown in Fig. 11.

The curves are drawn for the second vertical mode (two loops per span). In comparison with Fig. 10, at $\alpha_0 = 0$, there is a significant increase in the critical wind speed resulting from the effect of twisting. However, at the other values for α_0 there is actually a broadening of the range of instability compared with that of the untreated span, extending now up to 48 hm/h compared with 32 km/h. Thus, although it appears to help in one case, it hurts in the other two.

For the windamper, Fig. 12 shows that all three initial α_0 values are stable. There is one minimum in the damping curve at $\alpha_0 = 0$ and at 24 km/h, but it is offset by the combined damping of the line itself and by the windamper. *These curves demonstrate that the windamper's primary effect is through the twisting of the conductor which in effect uses the ice shape itself* to supply damping over certain portions of the span where C_α is positive, thus cancelling the effects o

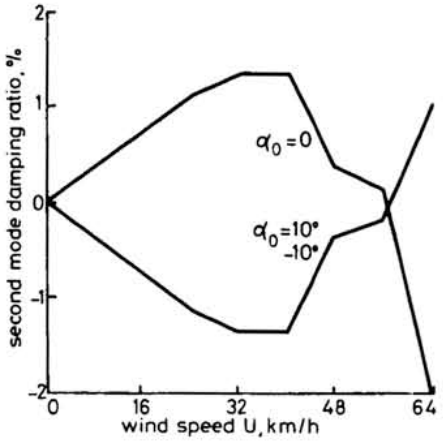

Fig. 11 *Detuner treated span damping ratio: second mode*
One detuner at each of the two 1/3-span points

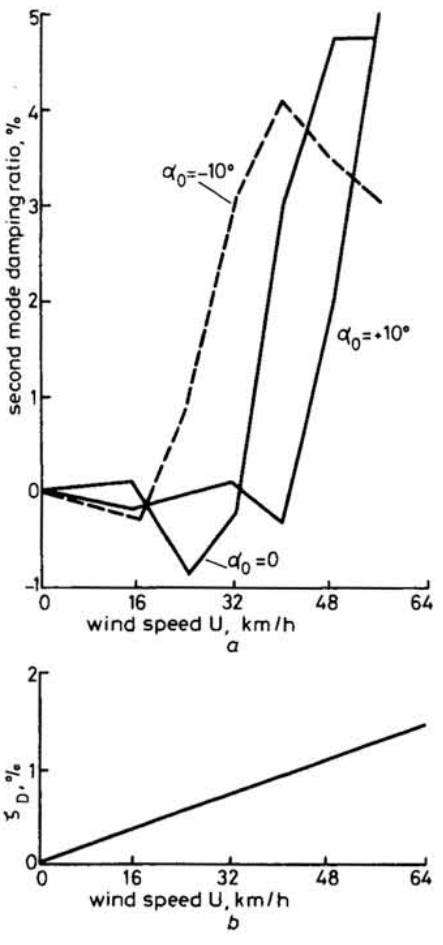

Fig. 12 *Windamper treated span damping ratio: second mode*
One damper at each of the two 1/3-span points
(*b*) Windamper contribution to damping, additive to curves in (*a*)

negative values on other portions. This explains why ordinary damping action, although helpful, cannot provide sufficient positive damping to overcome the ice shape's negative damping. Thus, damping action needs to be combined with twisting.

Another aspect to consider in the windamper is how the coupling action between the two modes (vertical and torsion) varies with wind speed. The way to find this out is to use the coupled eqns. 12 again, after having found the roots, and calculate, for each of the roots, the ratio between the y motion and the ϕ motion. These are called eigenvectors, Fig. 13.

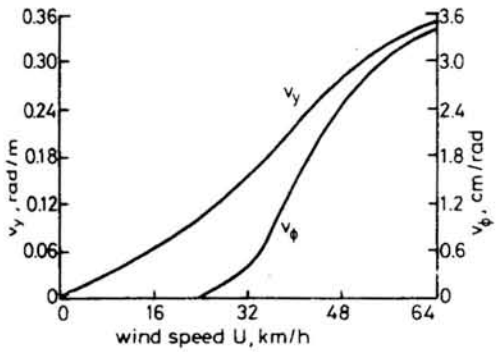

Fig. 13 *Windamper eigenvectors*

The eigenvector v_y indicates the influence of the second-mode motion on the windamper twist angle per unit displacement of the mode. At a wind speed of approximately 48 km/h twisting of $\pm 5^\circ$ is predicted. It appears to level off at higher wind speed. This twisting, found from the coupled eqns. 12 is primarily in phase with the vertical acceleration and does not affect the mode stability. It has, however, been incorrectly reported [1] as an instability of the damper itself. Actually, these observed motions at high wind speed are easily explained and accounted for by wind turbulence or wind gust effects. In this context, wind gusts are known to excite the span in its lower natural modes. When that happens, the windamper, being a part of the coupled dynamic system, becomes excited too. Since such twisting is spread uniformly along the span, it is considered harmless to the conductor.

The second eigenvector v_ϕ indicates the influence of the windamper dynamic twisting on the vertical motion of the span. This influence is quite small, requiring dynamic twist angles of one radian to produce only 2.5 cm displacement, at a wind speed of 48 km/h.

Actually, the dynamic twist motion produced by conductor displacement through v_y is considered beneficial when conditions exist for galloping. Although nonlinear effects have not been considered this far, the dynamic twisting through v_y will clearly drive the local angle of attack, especially near damper attachment points, into nonlinear ranges of the C_α characteristic, thus developing limit cycles at lower conductor amplitudes. This is another reason for not using heavy dampers.

7 Conclusions

Light ice develops galloping instability on untreated conductor spans when the initial angle of attack formed by the ice and the conductor blow back combine to develop negative aerodynamic coefficient, along the span.

A two-degrees-of-freedom analysis has been developed and applied to a typical span and three control devices, showing, on a comparison basis, the effects these devices have on the span under light-ice condition.

In comparison of the windamper and the perforated cylinder, the aerodynamic damping effect alone is insufficient to overcome the Den Hartog negative damping unless the size (span cover factor) is unreasonably large. This also explains why only modest reductions in galloping amplitude are predicted by an earlier theory [8]. The windamper twists the conductor as well, but the perforated cylinder does not. Twisting is shown to develop additional positive damping along the conductor span, leading to a stable system. Hence the windamper must be counted as a superior control device to the perforated cylinder.

Comparing the windamper and the detuner, no damping is introduced by the detuner whatsoever. Reverse twisting does occur for the detuner owing to its dead-weight pendulum effect. In two out of the three conditions studied, the reverse twist is degrading to the stability of conductor span. On the other hand, the windamper introduces additional positive damping on its own and also twists the conductor to stable angles of attack (see Figs. 11 and 12). Hence the windamper must be counted as a superior control device.

Comparing the detuner and the perforated cylinder, the detuner adds no damping on its own, but the perforated cylinder does. The reverse twisting of the detuner is helpful in delaying the onset of instability in one out of three cases, but degrading the stability in the other two (see Figs. 10 and 11). Hence the perforated cylinder damper must be counted as superior to the detuner.

The theory developed here takes into account the coupled vertical galloping motion to the torsional motion of the attached devices. It is a linear classical theory based on the solution of the coupled differential equations. In the illustrative example, neither the detuner not the perforated cylinder exhibits coupled motion, owing to negligibly small inertia offset (eccentricity). The windamper exhibits significant coupling of torsion to vertical motion, which is heavily damped (eqn. 6). The primary damper effect of the windamper is multiplied by its action in twisting the conductor statically, thus bringing into play a mixture of both stable and unstable angles of attack regimes along the span, the former tending to cancel the latter in achieving span stability.

These conclusions are generally valid for other span lengths, both longer and shorter, except that, on shorter spans, which have higher local torsion stiffness, some small increase in the suspension arm of the windamper may be required to ensure the large blow-out angle and attendant dynamic coupling action. Effects of either increasing or decreasing UBS have been investigated [11], and found to be small.

References

1 'Transmission line reference book: wind induced conductor motion'. Electric Power Research Institute, Project 792, 1980, Chap. 4, pp. 113–167

2 DELCOMMINETTE, A., HOFFELT, A., and COUVREUR, M.: 'Special electrical safeguard arrangements against galloping and similar phenomena on overhead lines'. CIGRE, 1974 Session, Paris, Paper 22–05

3 LEPPERS, P.H., BRAND, R., and COUVREUR, M.: 'Suppression of galloping for medium-size conductors by spacer removal or similar means'. CIGRE, 1978 Session, Paris, Paper 22–09

4 EDWARDS, A.T., and KO, R.G.: 'Interphase spacers for controlling galloping of overhead conductors'. IEEE Summer Power Meeting, Vancouver, BC, Proceedings of symposium on mechanical oscillations of overhead conductors, p. 101

5 RICHARDSON, Jr., A.S.: 'Design and performance of an eardodynamic anti-galloping device'. IEEE Summer Power Meeting, Chicago, I11., 1968, Paper 68Cp-670, also CIGRE, 1968, CSC-6-68-8

6 EDWARDS, A.T., and HOGG, A.D.: 'Control of galloping of overhead conductors by the "end-point" damping system'. IEEE Winter Power Meeting, New York, 1972, Paper CP72 185-2

7 HAVARD, D.G.: 'Detuning for controlling galloping of single conductor transmission lines, IEEE Summer Power Meeting, Vancouver BC, Proceedings of symposium on mechanical oscillations of overhead conductors, p. 87

8 HUNT, J.C.R., and RICHARDS, D.J.W.: 'Overhead-line oscillations and the effect of aerodynamic dampers', *Proc. IEE*, 1969, **116**, (11), pp. 1869–1874

9 Personal communications with windamper users (see also Reference 5, p. 9)
10 NIGOL, O., and BUCHAN, P.G.: 'Conductor galloping. Pt. II – Den Hartog mechanism', IEEE Summer Power Meeting, Vancouver BC, Proceedings of symposium on mechanical oscillations of overhead conductors, p. 26
11 RICHARDSON, Jr., A.S.: 'Some effects of conductor twisting on galloping, IEEE Summer Power Meeting, Vancouver BC, Proceedings of symposium on mechanical oscillations of overhead conductors, p. 34, also, *IEEE Trans.*, 1980, **PAS-99**, p. 811
12 RICHARDSON, Jr., A.S. and MARTUCCELLI, J.R.: 'Research study on galloping of electric power transmission lines'. MIT Progress Report 7, Nov. 1961, Aeroelastic & Structures Research Laboratory (see also Proceedings of conference on wind effects on buildings and structures, Teddington, England, June 1963, Paper 7, p. 612
13 EDWARDS, A.T.: 'Conductor galloping, *Electra*, Mar. 1970, (12), p. 31
14 ALDHAM-HUGHES, R.R., HERITAGE, C.A.R., ROWBOTTOM, M.D., and TUNSTALL, M.J.: 'Field monitoring of the performance of the CERL aerodynamic damper for controlling galloping', *in* 'Progress in cables and overhead lines 220 kV and above'. *IEE Conf. Publ. 176*, 1979, pp. 19–24
15 BROWN, G.S., and CAMBELL, D.P.: 'Principles of servomechanisms' (John Wiley & Sons, New York, and Chapman & Hall, London, fifth printing corrected, 1953), p. 90

9 Appendix: Physical description of the control device: concepts

Windamper

The windamper, shown in Fig. 1, is an aerodynamic damper consisting of paired back-to-back curved aluminum panels suspended by hanging brackets below the conductor attached rigidly to the conductor by inverted suspension clamps. The mass of the windamper is 10 kg, and its length is 1.22 m. Under no-wind condition it hangs directly below the conductor, but in a crosswind it blows out according to locally balanced aerodynamic deadweight and conductor torsion stiffness moments. It always contributes positive Den Hartog damping owing to aerodynamic drag and positive lift curve slope. The damping of the torsion mode of oscillation is similarly positive. The windamper has been developed in the USA by the present author.

Detuner pendulum

The detuner, shown in Fig. 2, is an inertia weight suspended below the conductor and attached rigidly to the conductor by its own clamp. Its offset centre of gravity and moment of inertia in combination with the local conductor torsion stiffness, create a torsion degree of freedom having a much lowered natural frequency as compared with either a bare conductor or a lightly iced conductor. It contributes no damping to the conductor on its own. Its deadweight eccentric moment resists local angle of attack changes otherwise caused by conductor blow back. Here, its weight and eccentric moment are put equal to that of windamper for purposes of comparing the two. The detuner has been developed in Canada by Ontario Hydro.

Perforated cylinder damper

The perforated cylinder, shown in Fig. 3, is an aerodynamic damper consisting of a round tube having a large number of holes on its surface for drag augmentation. Its Den Hartog damping is always positive but considerably less than that of the windamper for equal projected area. Its attachment to the conductor is symmetric producing no twisting. Here, a unit having the same weight as the windamper, but a length equal to 3.05 m yields approximately the same drag and conductor blow back as for the windamper. The perforated cylinder has been developed by CERL in Great Britain.